Constraining Emission Feature in the Range 85-115 MHz with MCMC

Raul A. Monsalve
raul.monsalve@colorado.edu

CASA, University of Colorado Boulder
SESE, Arizona State University

September 27, 2017

Here, we compute the region of parameter space favored/disfavored for a tanh emission feature with parameters a_{21}, z_r, and Δz over the frequency range 85-115 MHz. We use an integrated spectrum of Low-Band 1 data spanning the range 2015-288 to 2017-172, which includes Case 1 (original ground plane), Case 2 (extended ground plane), and Case 3 (extended ground plane after the receiver recalibration of May 2017).

We applied to all the datasets the receiver calibration done in May 2017 that produces calibration parameters up to 120 MHz. We used 7 polynomial terms to fit the noise wave parameters, and 8 terms to fit the scale and offset over 50-120 MHz.

This analysis should be considered a preliminary test. Since we did not have available a model for the beam with the original ground plane up to 120 MHz, we preferred not to apply beam correction in Case 1. We did apply beam correction in Cases 2 and 3. Other relevant aspects of the data and calibration are the following:

1. GHA range: 6-18 hr
2. Sun cuts: none (accepting day and nightime)
3. Moon cuts: EL $< 0^\circ$ for Cases 1 and 2. No cuts for Case 3, since there are not enough data for cuts.
4. Antenna S11: Case 1: 2015-342. Case 2: 2016-243. Case 3: 2017-153.
5. Losses: same balun and connector loss for all cases. 2% ground loss for Case 1. 0.5% ground loss for Cases 2 and 3.

The range 85-115 MHz was chosen because, at the low-end it connects with part of the absorption signature centered at $\approx$ 78 MHz. At the high-end, 117 MHz is the limit where the antenna S11 is still efficient, and where S11 measurement errors can still be tolerated. The 30-MHz range 85-115 MHz is also well modeled by 5 polynomial or physical terms. If the range is extended to lower or higher frequencies even by 1 MHz, it starts to require more foreground terms. This chosen range is also useful because it overlaps with the High-Band frequencies where we don't have strong constraints for an emission feature. In

fact, the average spectrum presented here has lower noise than the High-Band counterpart used in the paper Monsalve et al (2017) [1]. Finally, this range extends beyond the FM band (87-108 MHz) in both directions and, therefore, serves to evaluate the results of the RFI excision.

We tried other calibration options, such as antenna S11s different from the ones in the list above. However, they produce almost the same results when fitting the 85-115 MHz range with 5 foreground terms.

The MCMC approach attempted here differs from the model rejection method in Monsalve et al. (2017) in that here we estimate all the parameters, including the non-linear 21-cm parameters z_r and Δz, simultaneously. The uncertainties derived for each parameter account for covariances with the other parameters. The measurement noise assumed in the MCMC has a frequency-independent standard deviation of 10 mK, equal to the RMS of the residuals to a 5-term polynomial fit.

The analysis and results are summarized in the following figures:

- Figure 1 shows the three antenna reflection coefficients used for each of the datasets, in the range 85-115 MHz.
- Figure 2 shows the residuals of the integrated spectrum to a polynomial and physical model fit with 5 terms over 85-115 MHz.
- Figure 3 shows MCMC results for z_r and Δz when fitting a tanh model with an amplitude of $a_{21} = 1$ mK and 10 mK.
- Figure 4 shows MCMC results for z_r and Δz when fitting a tanh model with an amplitude of $a_{21} = 28$ mK and 50 mK.
- Figure 5 shows MCMC results for z_r and Δz when fitting a tanh model with an amplitude of $a_{21} = 100$ mK.
- Figure 6 shows MCMC results for a model with $a_{21} = 28$ mK and fit parameters z_r and Δz, after injecting an artificial signal with $a_{21} = 28$ mK, $\Delta z = 0.3$, and two values for z_r, 15 and 14.
- Figure 7 shows MCMC results for a model with $a_{21} = 28$ mK and fit parameters z_r and Δz, after injecting an artificial signal with $a_{21} = 28$ mK, $\Delta z = 0.3$, and two values for z_r, 13 and 12.
- Figure 8 shows MCMC results for the three fit parameters, a_{21}, z_r, and Δz using just the original measurement, as well as measurement plus an injected signal.

Conclusions

1. The frequency range examined here includes the 'knee' of the absorption signature between ~ 85 and 90 MHz. This results in a 'detection-like' feature at $z \approx 14.5$ in the MCMC posterior distributions. In the future, we could try this analysis focusing on rejecting EoR transitions only above 90 MHz to simplify the interpretation of the results.
2. The two foreground models (EDGES polynomials and physical model) produce different patterns for the favored/disfavored regions, except for the 'knee' mentioned above which in general is identified with both models, especially when the tanh amplitude is fixed.

[1] Monsalve, R. A., Rogers, A. E. E., Bowman, J. D., Mozdzen, T. J., 'Results from EDGES High-band. I. Constraints on Phenomenological Models for the Global 21 cm Signal'. ApJ 847, 64, 2017

3. When the tanh model amplitude is fixed at $a_{21} = 28$ mK, models can be rejected with durations up to about $\Delta z \approx 0.5$ over a significant fraction of the range $15.5 \gtrsim z \gtrsim 11.5$, except for the region of the knee.

4. When a tanh signal is injected and then estimated assuming the same (correct) fixed amplitude, the recovery is accurate except around $z \approx 15$, possibly due to the interaction between the knee in the real data and the artificial injected signal.

5. When the three 21-cm parameters (a_{21}, z_r, and Δz) are fitted to the data, only using the EDGES polynomial produces meaningful constraints. However, when a strong (60 mK) tanh signal is injected to the data, the physical model recovers it with higher precision. These cases show the difficulty in determining which foreground model is the best.

6. In the next iteration of this analysis we can try to reduce the noise of the integrated spectrum by accepting data with the Moon above the horizon, up to, for instance, 30°, instead of using the current limit of 0°.

7. For consistency, in the future we should also apply beam correction to data from Case 1, which for this report was not done.

8. Finally, we should also calibrate the data with the recent receiver calibration conducted at ASU in September 2017.

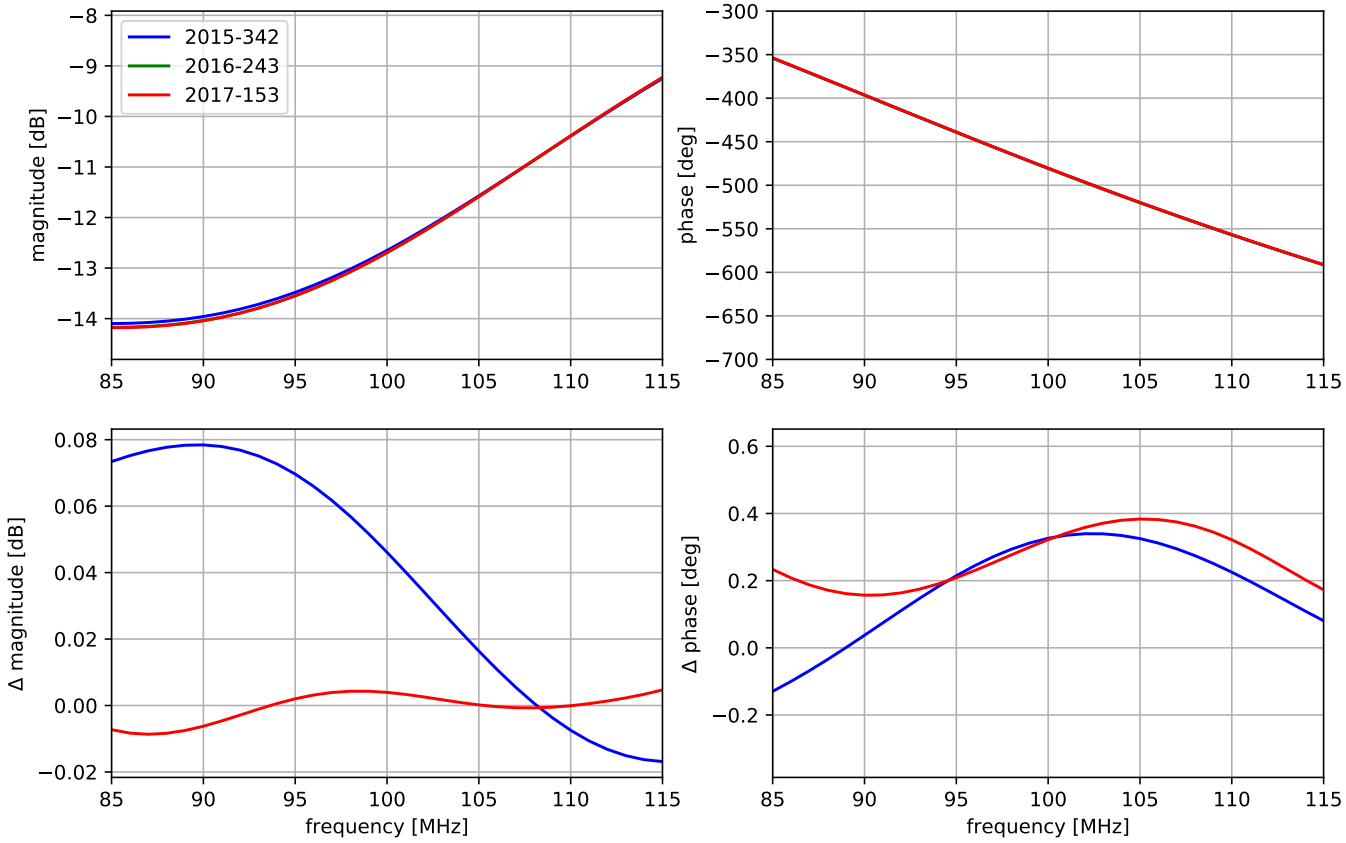

Figure 1: (Top) Antenna reflection coefficients (s11) used to calibrate data from Case 1 (2015-342), Case 2 (2016-243), and Case 3 (2017-153). Red and green lines overlap on these scales. (Bottom) Difference of s11 from Case 1 and Case 3, relative to Case 2.

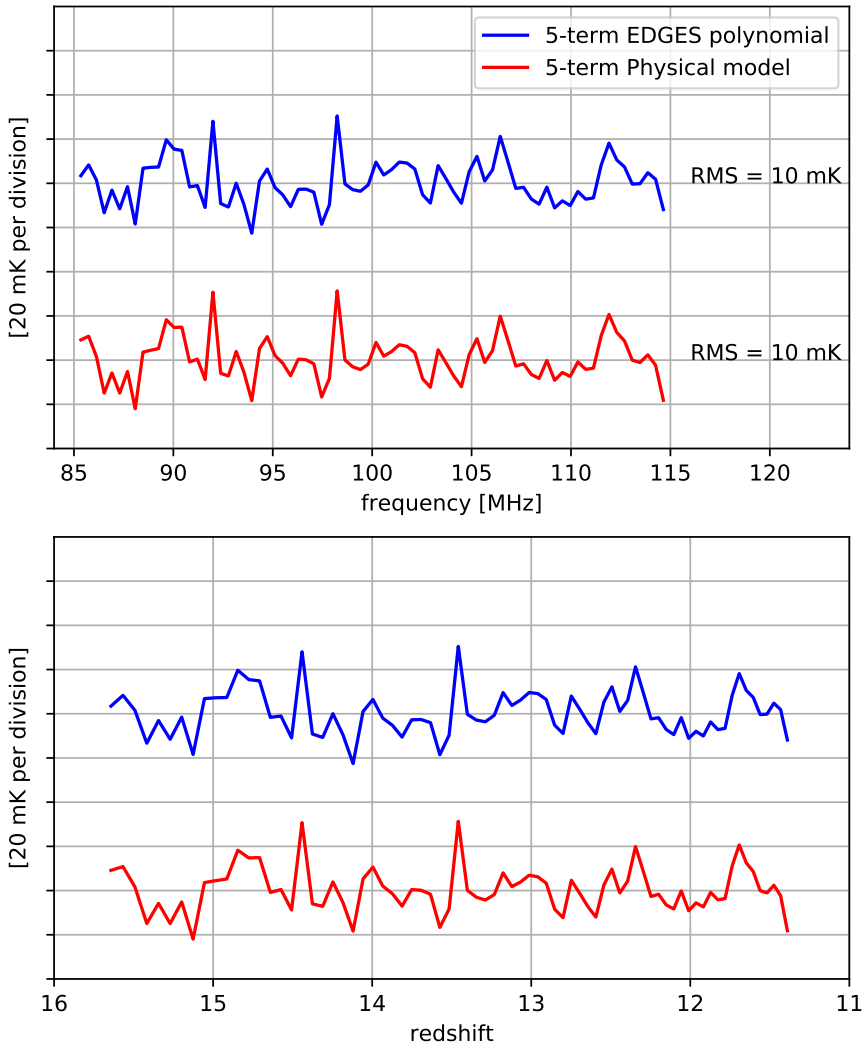

Figure 2: (Top) Residuals of the integrated spectrum to a 5-term EDGES polynomial and a 5-term physical model. (Bottom) Same residuals but as a function of redshift. There are a couple of spikes that might be due to RFI, which could be removed in a more refined analysis or mitigated by using more data in the integrated spectrum. It is also possible to identify, barely above the noise, two humps in the residuals from both foreground models, especially in the bottom panel: one hump centered at ≈ 90 MHz ($z \approx 15$) and one at ≈ 105 MHz ($z \approx 12.5$). The first hump is part of the main absorption signature, while the second one could be the result of potential calibration inaccuracies.

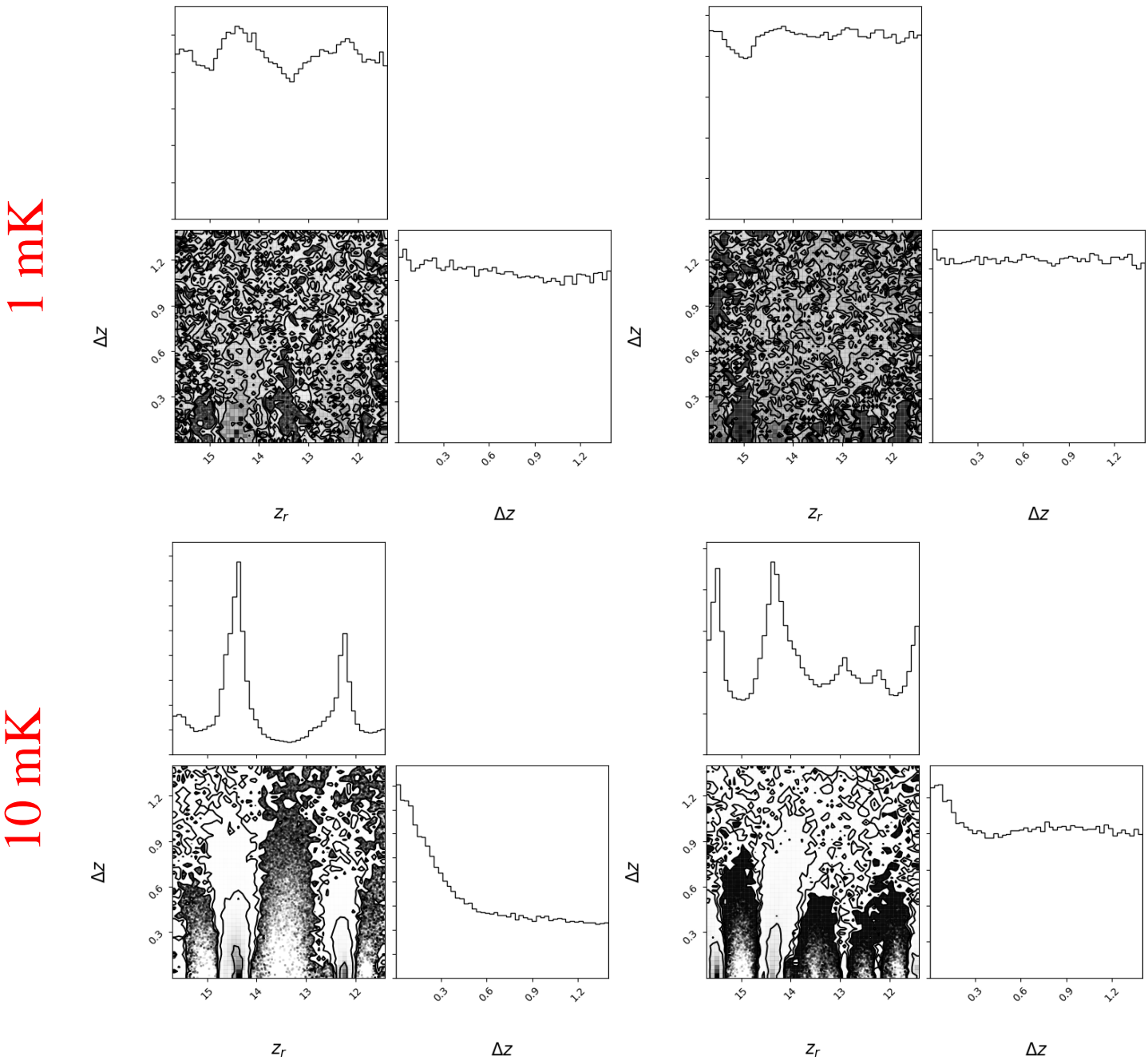

Figure 3: (Top) MCMC results when estimating a tanh model with a fixed amplitude of 1 mK, using both foreground models (two columns). As expected, there are no constraining capabilities for such a small signal. This computation was done as a sanity check. (Bottom) MCMC Results when estimating a tanh model with a fixed amplitude of 10 mK. Regions with lower and higher likelihood are more clearly identified. In particular, with the polynomial model (left), two 'tanh-like' descending slopes can be identified, centered slightly below $z \approx 14.5$ and $z \approx 12.5$.

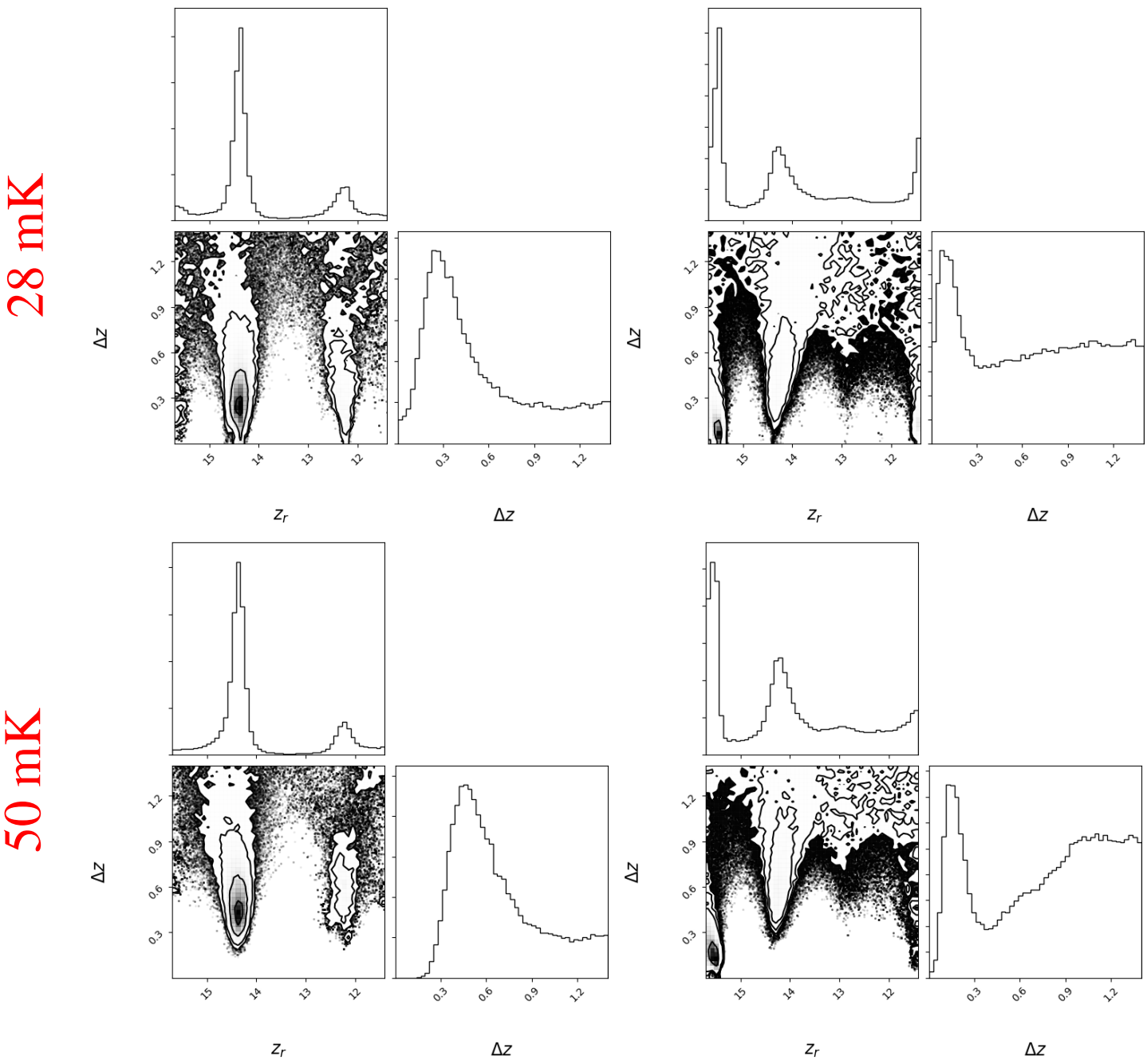

Figure 4: MCMC results when estimating a tanh model with a fixed amplitude of 28 mK (top) and 50 mK (bottom). The descending slope at $z \approx 14.5$ is more strongly identified with both foreground models. There are large regions where sharp transitions can be ruled out.

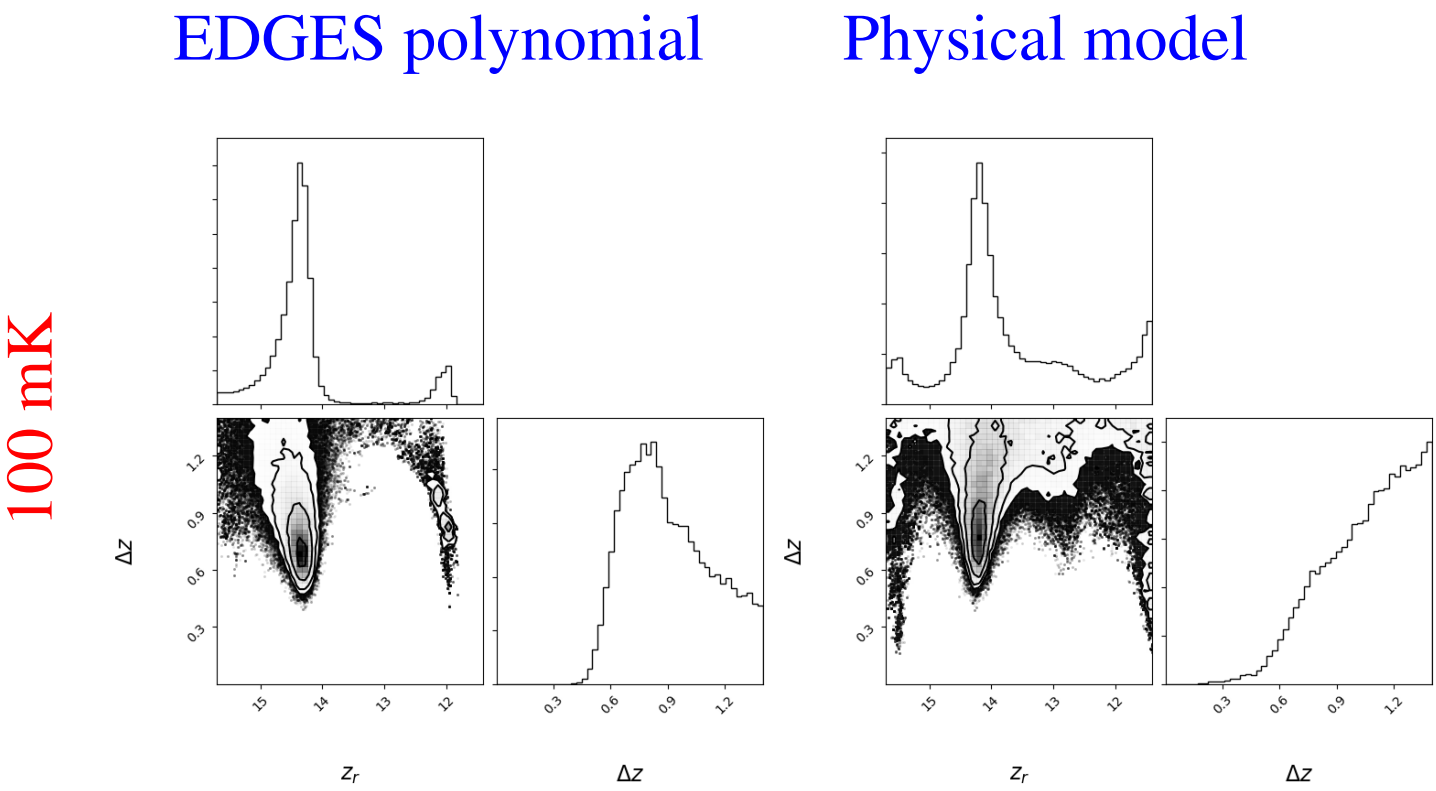

Figure 5: MCMC results when estimating a tanh model with a fixed amplitude of 100 mK. The descending slope at $z \approx 14.5$ remains strongly identified but with a larger duration ($\Delta z \gtrsim 6$) than for smaller amplitudes (see previous figues). As expected, for this amplitude there is a larger disfavored/ruled out region.

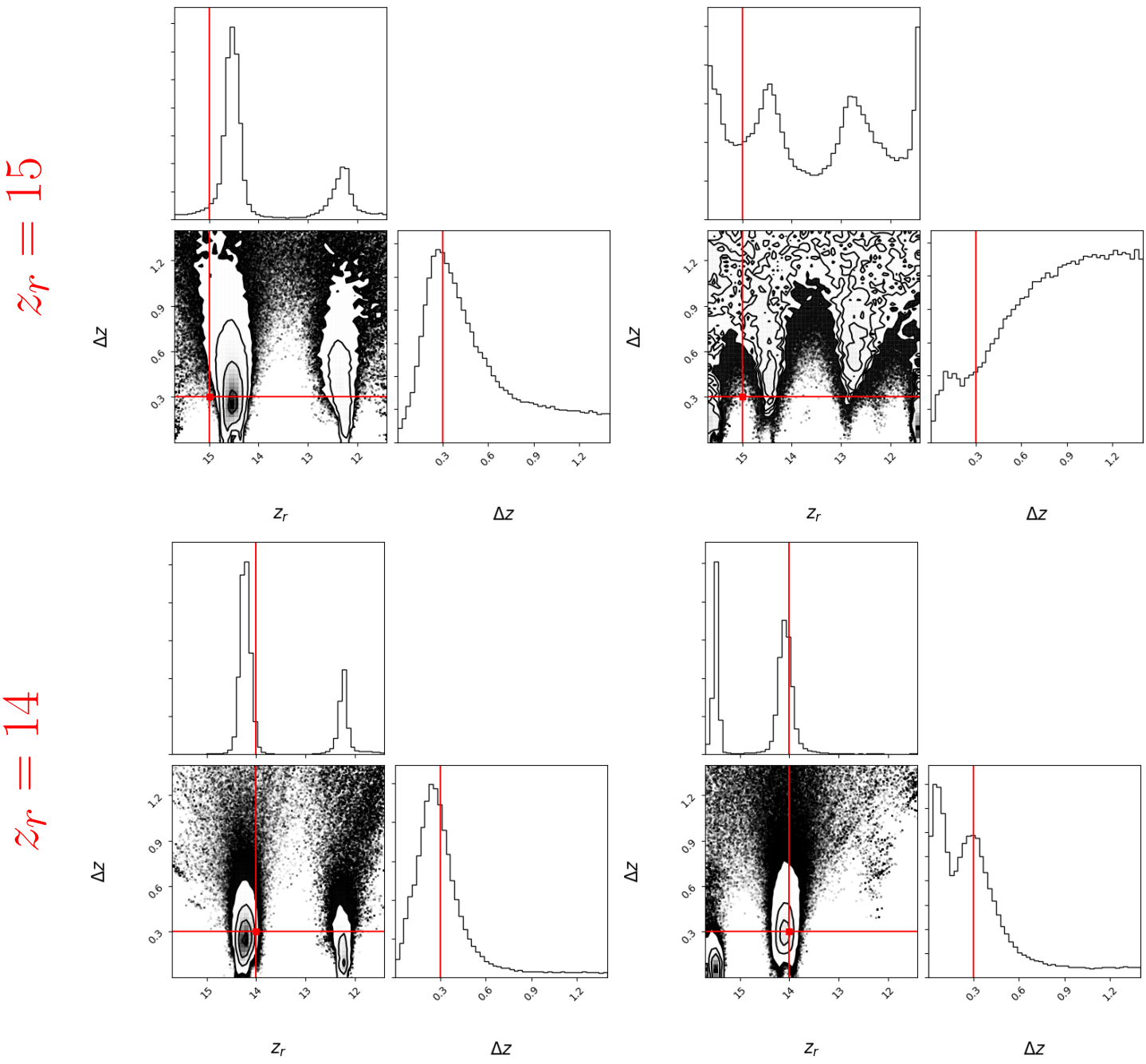

Figure 6: MCMC results after injecting a 28-mK tanh with duration $\Delta z = 0.3$ centered at different redshifts (red square). The model assumed by the MCMC also has a fixed amplitude of 28 mK. (Top) The injected signal is centered at redshift $z_r = 15$. (Bottom) The injected signal is centered at redshift $z_r = 14$. For $z_r = 15$, the recovery of the injected signal is not as accurate as expected, possibly due to the interaction of the injected signal with the hump in the actual data.

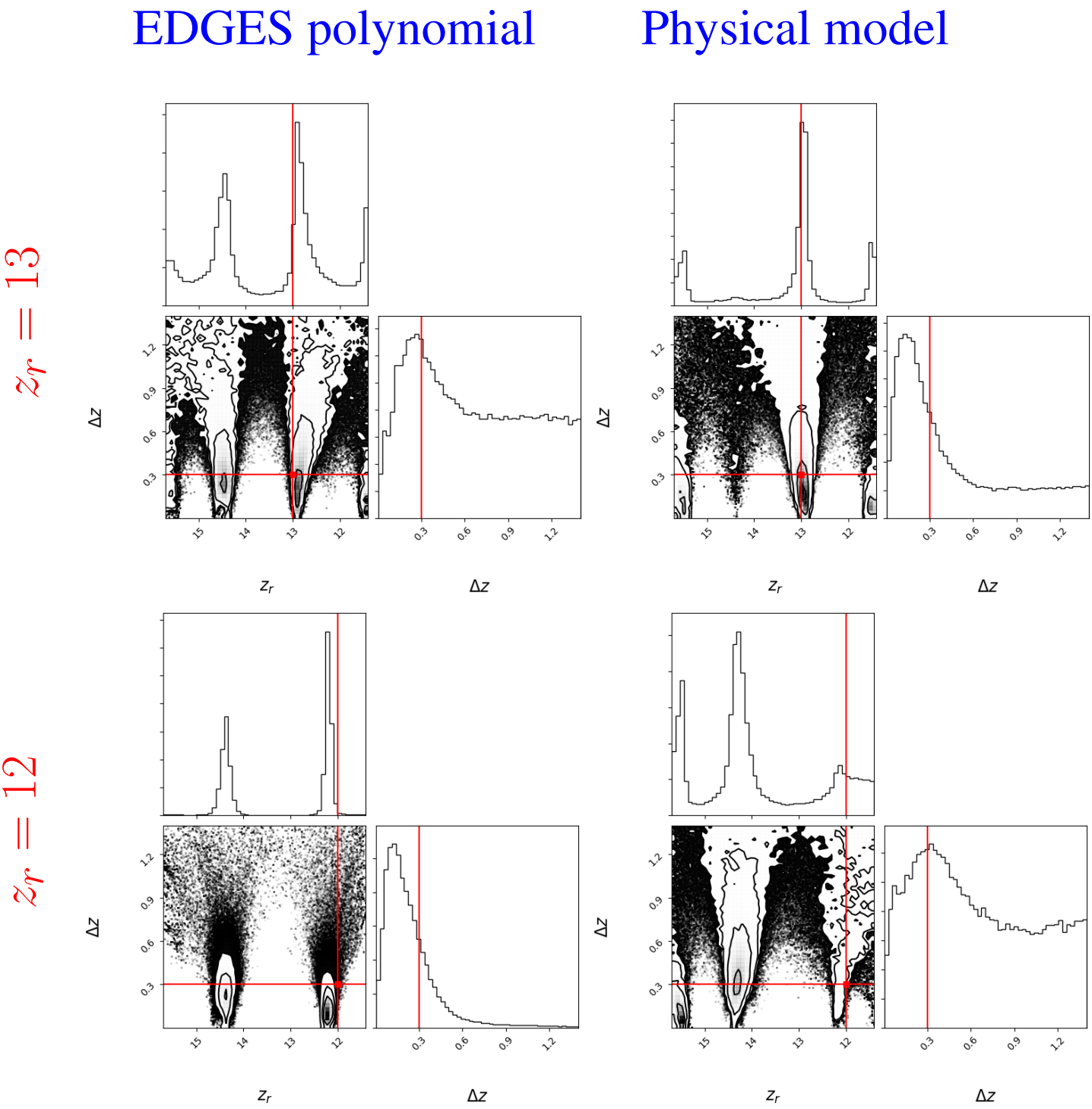

Figure 7: MCMC results after injecting a 28-mK tanh with duration $\Delta z = 0.3$ centered at different redshifts (red square). (Top) The injected signal is centered at redshift $z_r = 13$. (Bottom) The injected signal is centered at redshift $z_r = 12$. In both cases the recovery of the injected signal is adequate and, at least in three of the cases shown here, the MCMC also maintains the identification of a hump in the real data at $z_r \approx 14.5$.

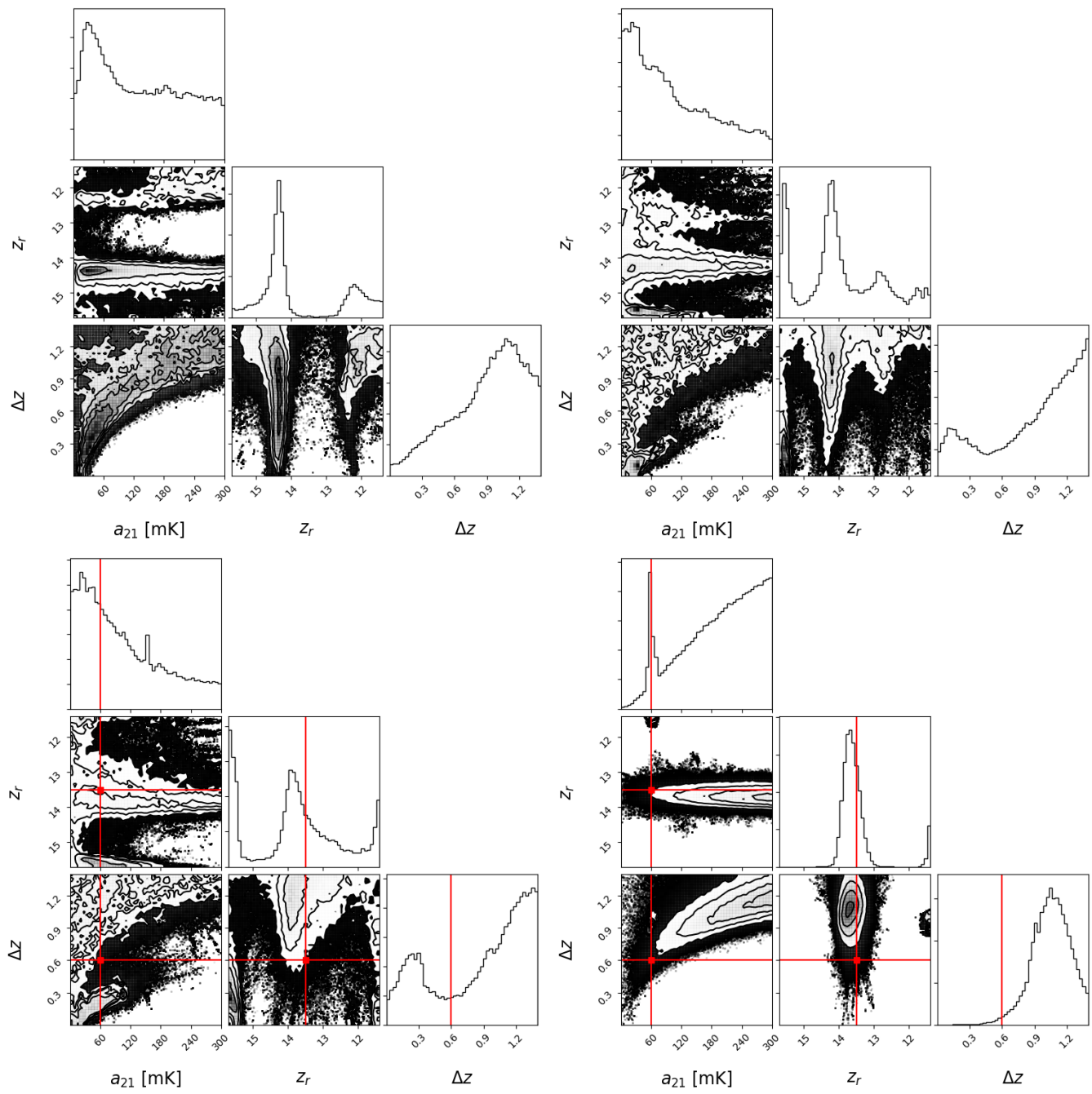

Figure 8: (Top) MCMC results for the three 21-cm fit parameters, a_{21}, z_r, and Δz. With the EDGES polynomial foreground model (left), the highest probability region is around $a_{21} = 40$ mK, $z_r = 14.5$, $\Delta z = 0.4$. With the physical model (right) the region is not clearly identified. Only the center redshift is estimated with above-average probability, to be $z_r \approx 14.5$. When using the EDGES polynomial it can be concluded that, in the range $14 \gtrsim z \gtrsim 12.5$, amplitudes $a_{21} > 80$ mK and durations $\Delta z < 0.5$ are disfavored (independently, after marginalization). (Bottom) MCMC results after injection of artificial tanh model with $a_r = 60$ mK, $z_r = 13.5$, and $\Delta z = 0.6$. This 'true' value is depicted with the red square. Although the MCMC distributions with both foreground models are consistent with the injected signal, using the physical model (right) produces more compact and better defined distributions than the EDGES polynomial (left). Still, even for the relatively large injected signal of $a_{21} = 60$ mK, the fitting of three parameters (in addition to the five polynomial terms) does not produce precise estimates in this context. In general, the interaction between the 'knee' in the actual data and the artificial signal injected complicates the interpretation of the results.